Processing ground penetrating radar (GPR) data

Steven C. Fisher*, Robert R. Stewart, and Harry M. Jol†

ABSTRACT

Two ground penetrating radar (GPR) profiles provided by the University of Calgary, Department of Geography are analyzed using seismic data processing techniques. The first is a 120m, 100 MHz, single-fold line from Ft. Smith, N.W.T. Processing operations performed on this data include signal saturation, gain recovery, spiking deconvolution, bandpass filtering, and normal moveout corrections. A failure surface with no surface expression is recognized in the final section. The second profile is a single-fold, 50 MHz, 0.5km line from William's Delta on Lake Athabaska, Saskatchewan, showing deltaic crossbed structures. These were processed using similar steps as above as well as f-k migration.

The filter bandwidths chosen from the 50 MHz and 100 MHz amplitude spectra were 20/30 - 70/100 MHz and 20/30 - 100/125 MHz respectively, suggesting very rapid attenuation of higher frequencies. A velocity spectrum was made for Williams Delta based on groundwave first arrivals and a common midpoint (CMP) gather velocity semblance analysis. Based on an average radar velocity of ~0.07m/ns, the William's Delta lithology was determined to be a water saturated fine sand. Analogous to seismic reflectivity, the GPR reflection coefficient is dependent on the dielectric contrast accross an interface. Two higher velocity surface layer statics are recognized in the William's Delta profile. An attempt was made to correct these by flattening a water - table reflection. This was found to be insufficient, so a static correction formula was derived.

INTRODUCTION

Ground penetrating radar (GPR) has gained popularity as a shallow subsurface, geophysical imaging tool due to its ease of use and portability for recording high resolution sections. GPR has a range of applications in archaeology, engineering, and the earth sciences such as "delineating the water table depth, frozen-unfrozen interfaces, mapping soil stratigraphy, subsurface bedrock topography, peat deposits, geological structure, and locating buried pipes, cables," (Jol and Smith, 1991) and ordnances (Hogan, 1988).

GPR is a technique that transmits pulsed electromagnetic waves (10 - 1000 MHz) which can be refracted and/or reflected off subsurface features, received, and recorded digitally in a manner similar to seismic surveying techniques. However, many of the problems affecting seismic signals also affect GPR. Therefore, assuming electromagnetic waves propagate analogously to elastic energy, seismic data processing techniques are for GPR. This is a reasonable assumption for propagating radar wave traveltimes.

* University of Calgary, geophysics undergraduate student
† University of Calgary, Department of Geography

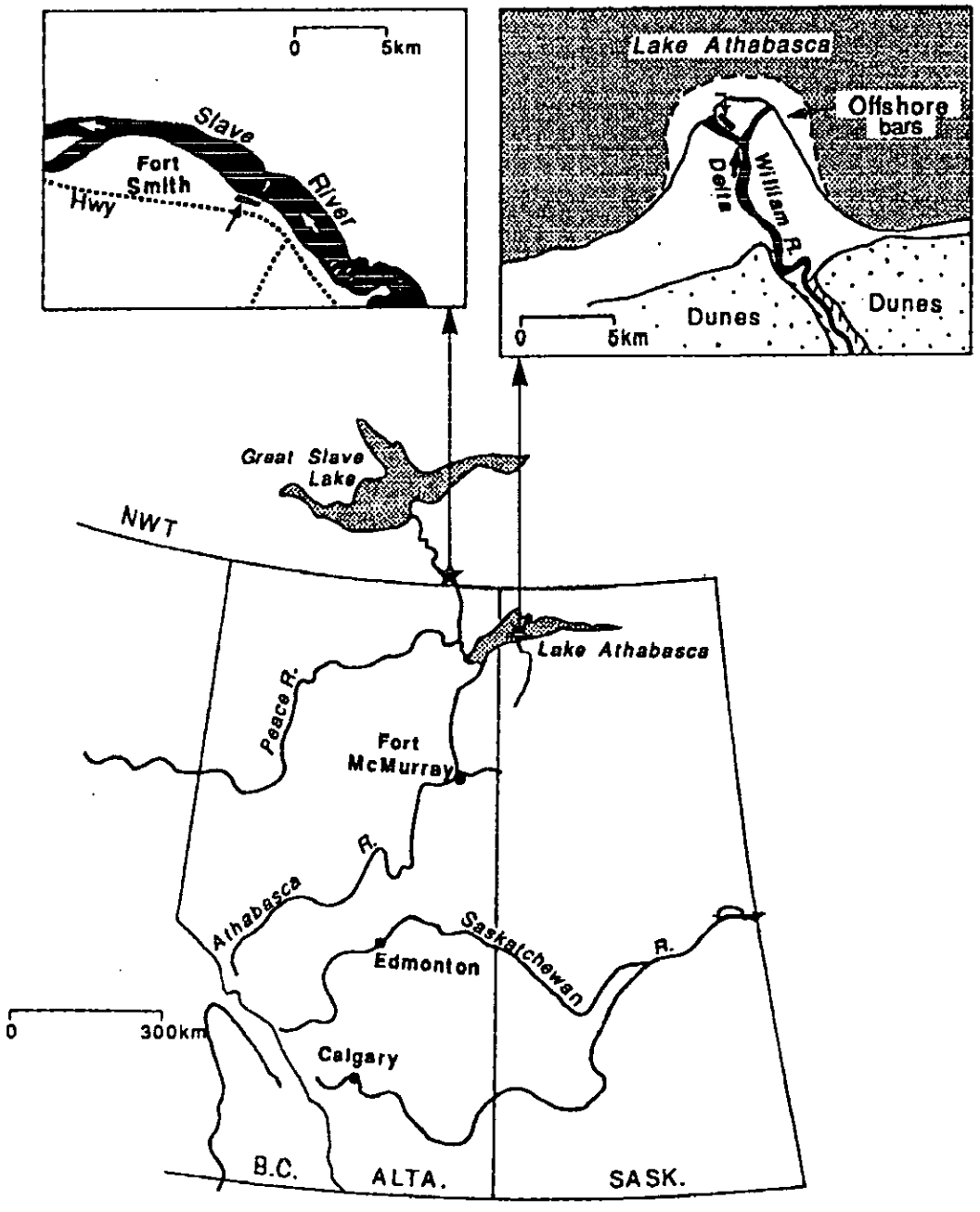

FIG. 1. Locations of GPR data sets recently acquired by Jol and Smith (1991). Slave River (top left) and William's Delta (top right). Diagram modified from Jol and Smith (1991).

EQUIPMENT

The data for this project were provided by the University of Calgary, Department of Geography, who own and operate an advanced, high-fidelity (or high signal-to-noise), digitally recording pulseEKKO IV GPR acquisition system (manufactured by Sensors and Software Inc., Mississauga, Ontario). It operated here with a 400V pulser voltage. Each output trace consisted of a 64-fold vertical stack.

The VISTA 6.5 seismic processing package was used with the signal dewowing (DC offset / signal saturation correction) program in the pulseEKKO IV operations software. Migration and hardcopy displays were created using Inverse Theory and Applications software on a SUN Sparcstation workstation.

STUDY AREAS

The first data set is a 100 MHz, 120 trace line from Slave River Delta, Fort Smith, Northwest Territories (Figure 1). The geometry consisted of a single-fold, constant 1m antenna separation, with 1m shot interval (or step size). The processed single-fold data are shown in Figure 2. This line displays a distinct failure plane that was reported by Jol and Smith (1991) to have no surface expression.

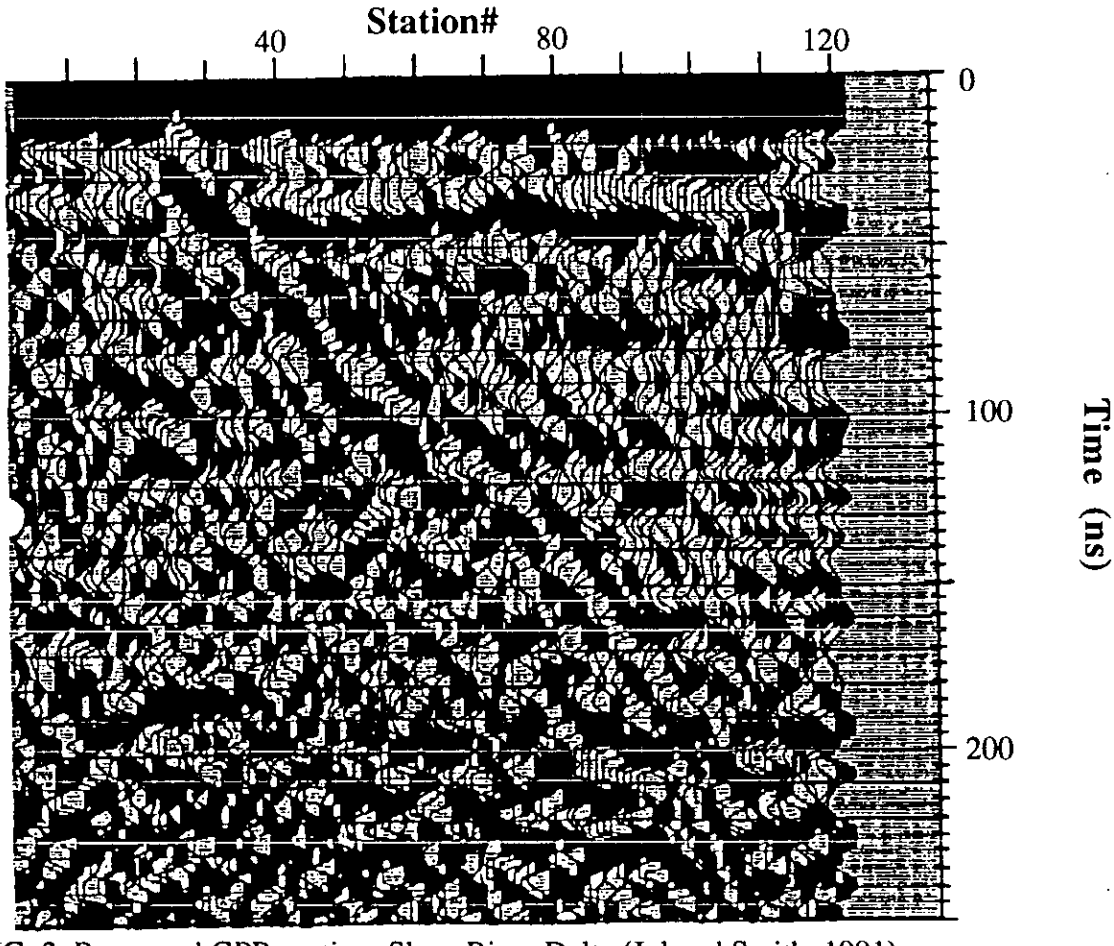

FIG. 2. Processed GPR section: Slave River Delta (Jol and Smith, 1991).

The second data set is a 50 MHz profile, with CMP gather, from William's Delta on the south shore of Lake Athabaska, Saskatchewan, showing steeply dipping foreset beds in a water saturated environment, and a sharp bottom boundary. The geometry here consisted of a 2m antenna separation with 1m step size.

PROCEDURE AND THEORY

Figure 3 shows the processing flow used for analyzing the GPR data. First, raw data (Figure 4) are corrected for signal saturation effects using the pulsEKKO IV system software. After a spherical divergence correction, the data were spiking deconvolved then bandpass filtered on VISTA 6.5. Zero-phase and predictive deconvolutions were not successful. Then after flattening the airwave, obvious static busts were corrected for by approximating the water-table depth and near surface radar velocities. Once electromagnetic radar velocities are determined, normal moveout is performed on each trace to correct for transmitter / receiver antenna separation. Finally, the data were f-k migrated to better approximate the real structure.

Signal saturation

Figure 5(a) shows the DC offset and signal saturation corrections. Because of the large energy input from the airwave, groundwave, and near surface reflectors, the GPR receiver becomes signal saturated and unable to adjust fast enough to the large variations between vertical stacks. This induces a low frequency, slowly decaying "wow" on the higher frequencies of the signal trace arrivals, making arrivals on the shaded wiggle traces tough to distinguish. DC signal saturation is constant across each trace and can be corrected for by a bulk DC offset shift in amplitude towards zero. The final correction is an optimal low - cut filter determined by Sensors and Software Inc (1989) (Figure 5(b)).

Gain recovery

Due to geometrical spreading of transmitted wavefields, later arrivals on a signal trace show noticeably lower amplitudes than earlier arrivals (Figure 4). To recover relative amplitude information, a time - variant, trace equalization function such as spherical divergence (equation 1) or automatic gain control (AGC) is applied (Figure 6). The spherical divergence exponential gain constant(n) used here is 50:

$$b_i[j] = i * a_i[j] * e^{i*n*\frac{dt}{10000}} \qquad (1)$$

Where $a_i[j]$ is the ith sample of the original amplitude trace a[j], $b_i[j]$ is the ith sample of the gain recovered trace b[j], and dt is the sample rate (0.8ns).

Spiking deconvolution

Spiking wavelet deconvolution (40 ns operator window and 1% prewhitening) vs zero-phase deconvolution was found, by trial and error, to best enhance the resolution of the data when followed by a bandpass filter (Figure 7). Predictive deconvolution was also attempted but failed to remove the primary multiple at ~850ns (Figure 6).

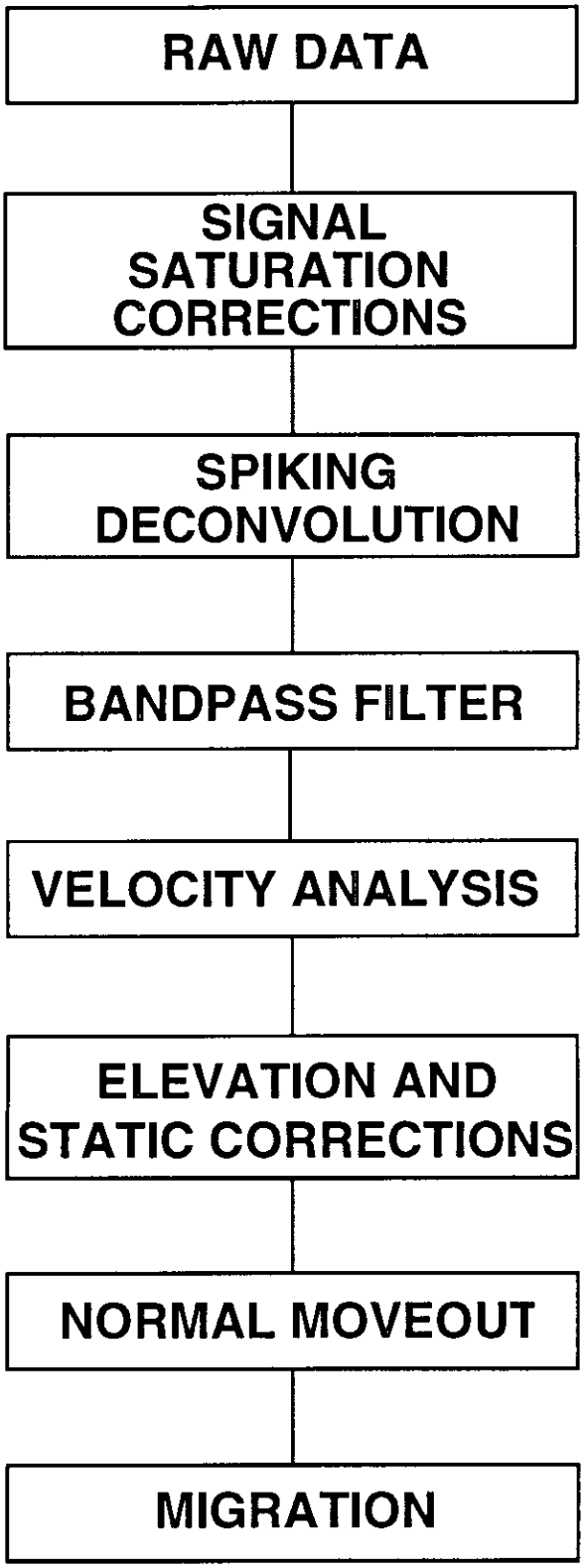

FIG. 3. GPR processing flow.

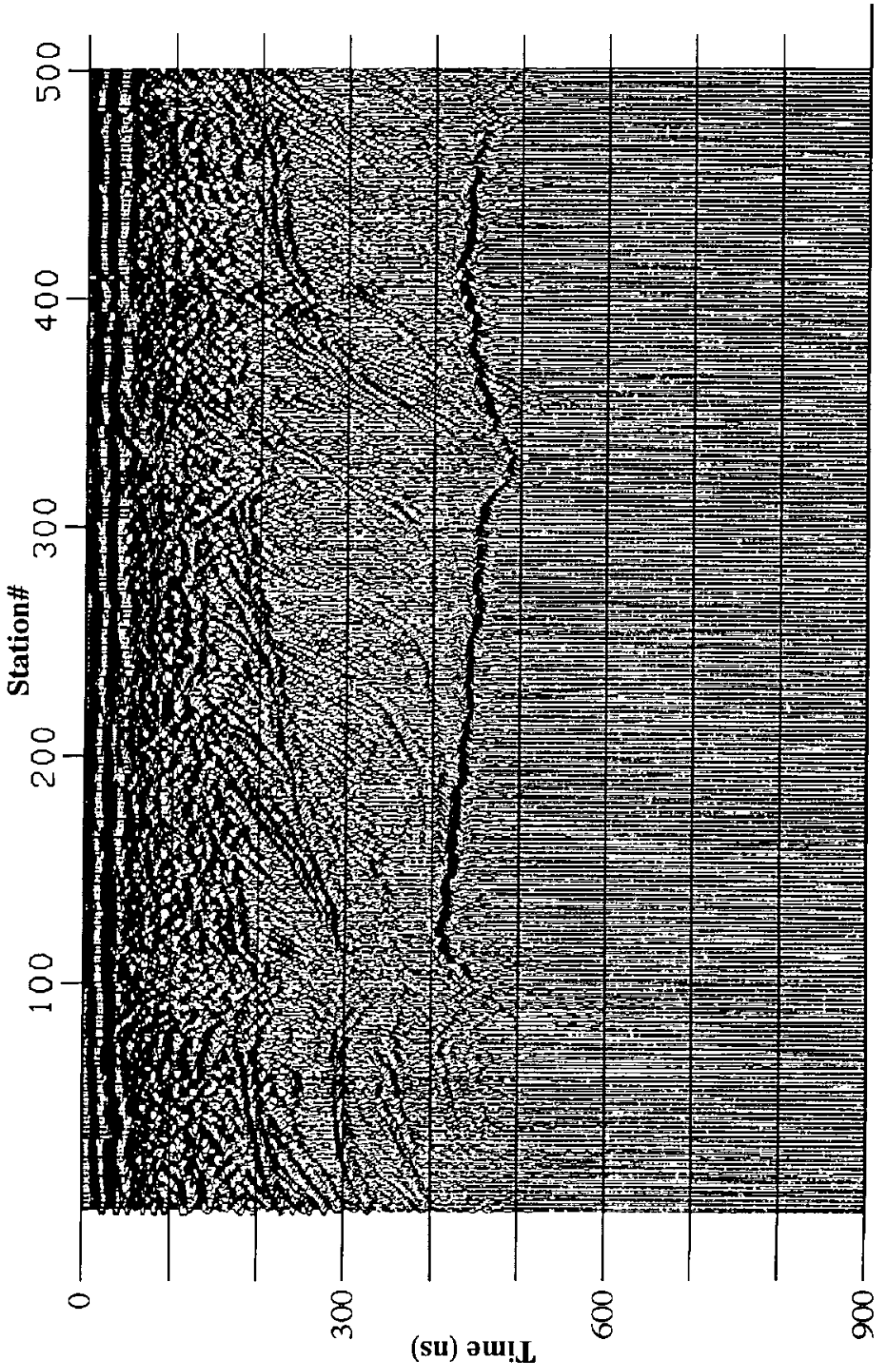

FIG. 4. Raw Data.

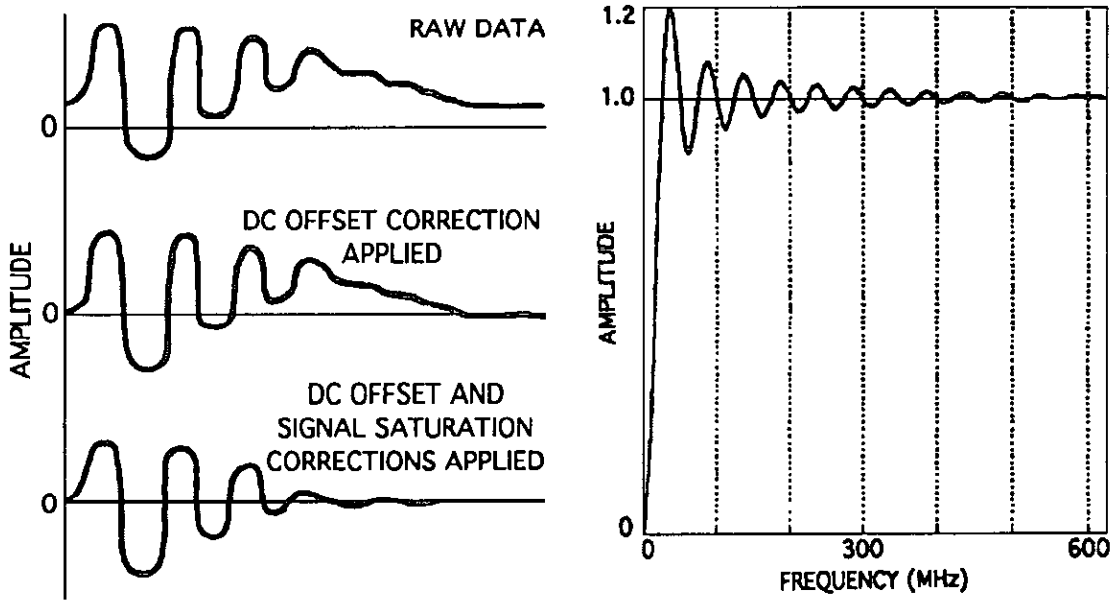

(a) (b)

FIG. 5. (a)DC offset and signal saturation corrections (Moorman, 1990). (b) Signal saturation correction low - cut filter amplitude spectrum.

Bandpass filter

Amplitude spectra were plotted by Vista 6.5 for each trace and summed to determine the signal frequency bands of the 50 MHz (William's Delta) and 100 MHz (Slave River Delta) GPR data sets (Figure 8). According to Davis and Annan (1989) "G.P.R. systems are designed to achieve bandwidths that are about equal to the center frequency." For the 100 MHz data rapid attenuation of frequencies greater than 75 MHz was observed (Figure 8(a)). The frequency bands chosen for filtering were 20/30 - 70/100 and 20/30 - 100/125 MHz for the 50 and 100 MHz transmitter bandpass filters respectively.

Velocity analysis

A common midpoint (CMP) gather (Figure 10) was aquired by Jol and Smith (1991) at William's Delta adjacent to where the profiling survey was acquired (Figure 4) using the Figure 9 spread geometry. From an initial 19m seperation, the antenna converged towards the CMP (trace #39) at 0.25m steps, crossed at the CMP and seperated until the final record trace #78. Thus, each record trace respresents a 0.5m change in antenna seperation. This CMP gather is therefore assumed to indicate the approximate electromagnetic wave velocity-depth spectrum throughout the William's Delta section.

The airwave is the first radar signal to reach the receiver travelling at the speed of light (0.30 m/ns (Figures 11 and 12)). Knowing this is useful for fighting GPR system fibre-optic recording problems by flattening the airwave to the time:

$$t = \frac{\text{antenna separation}}{0.30\text{m/ns}} . \qquad (2)$$

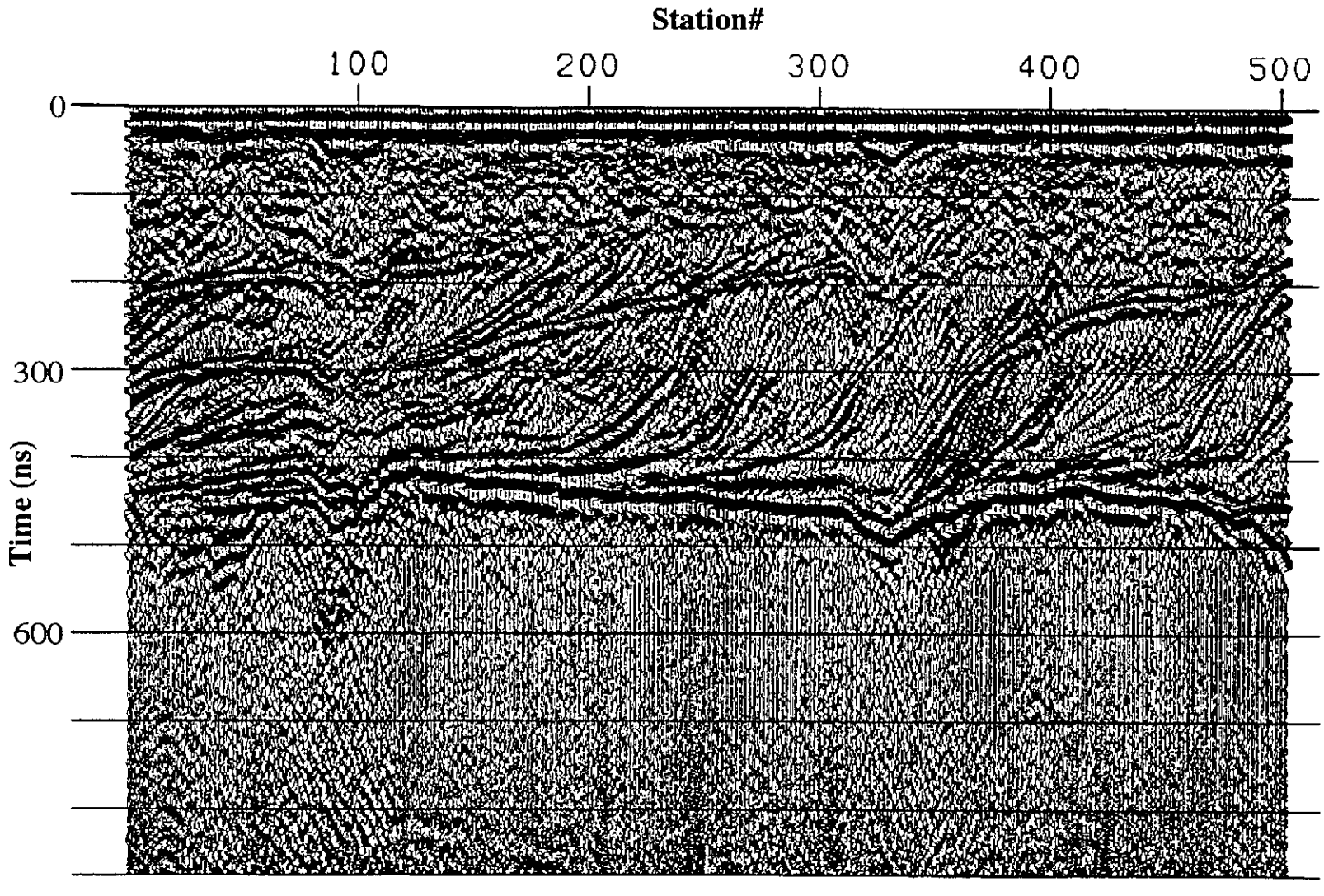

FIG. 6. Signal saturation corrections, airwave flattening, and gain recovery.

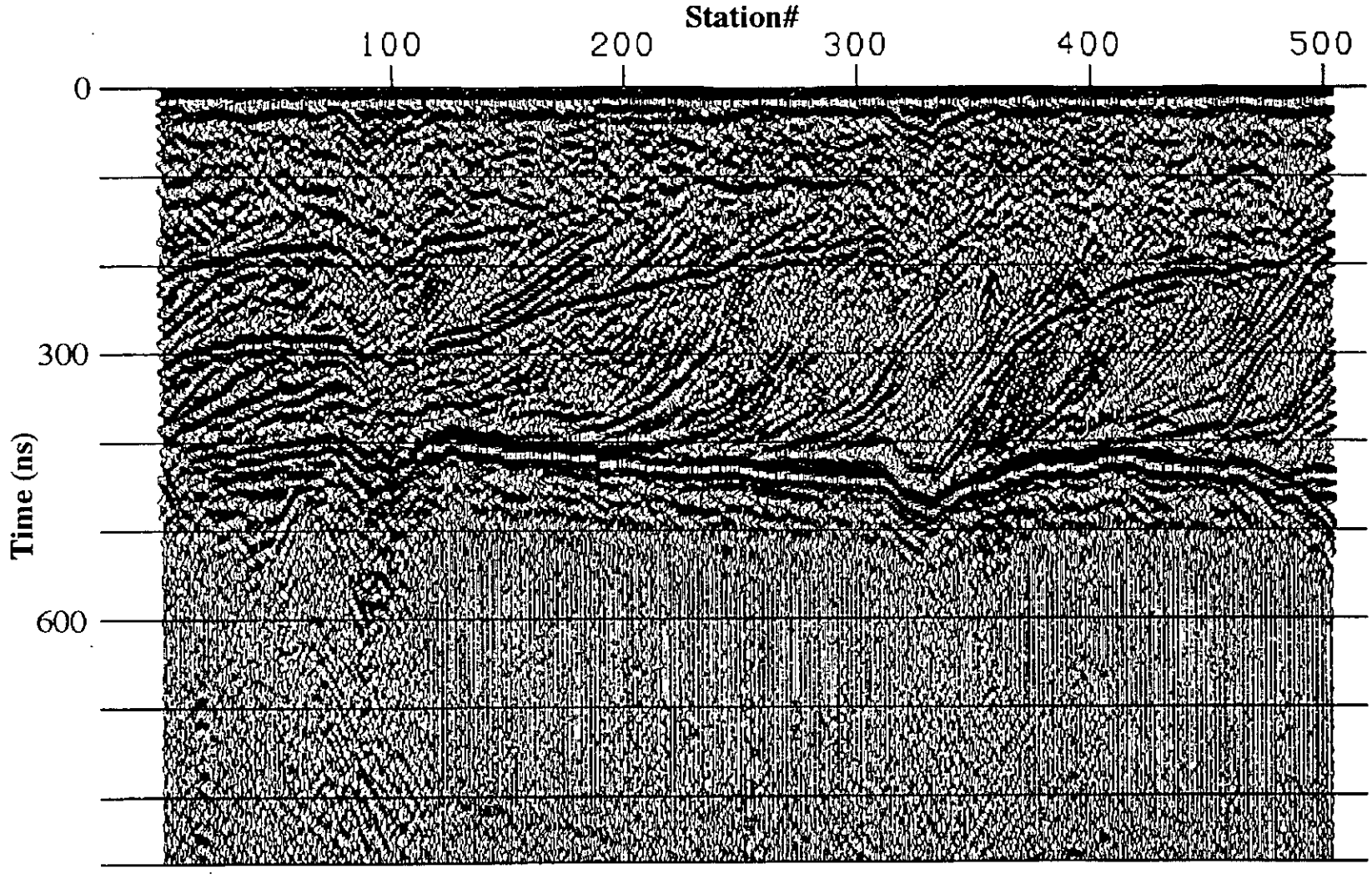

FIG. 7. Spiking deconvolution and bandpass filter (20/30 - 70/100).

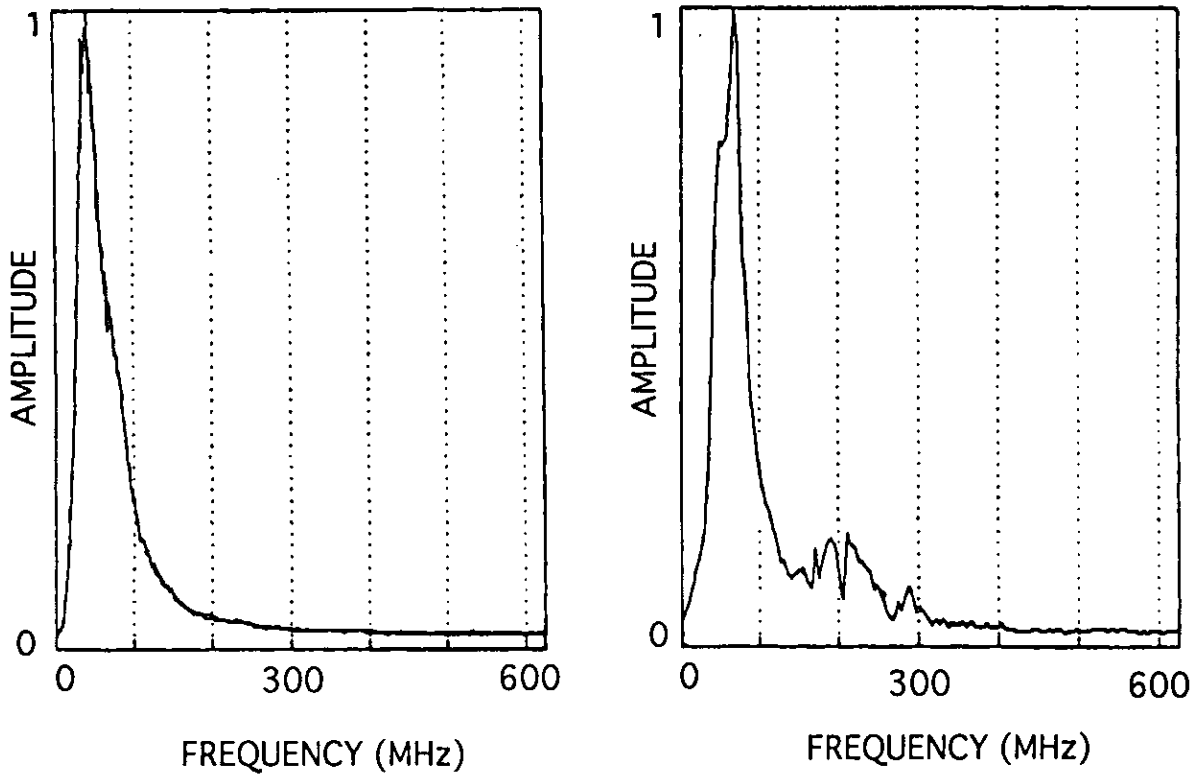

(a) (b)

FIG. 8. Summed amplitude spectra of the (a)50 MHz William's Delta and (b)100 MHz Slave River Delta GPR data sets.

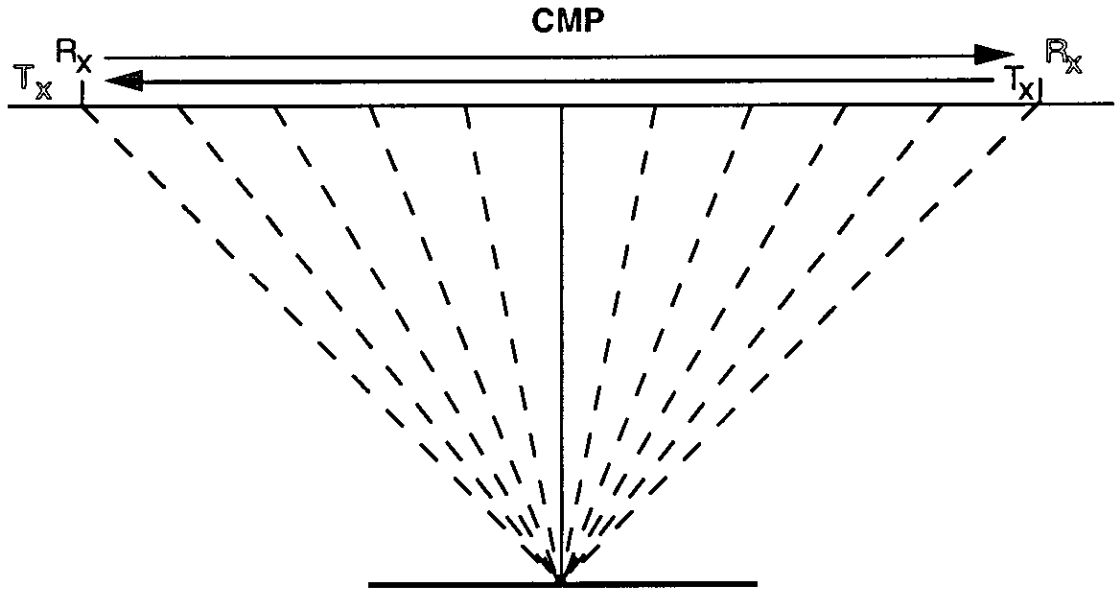

FIG. 9. Common midpoint (CMP) spread geometry. 0.25m station spacing and 0.5m antenna seperation per trace.

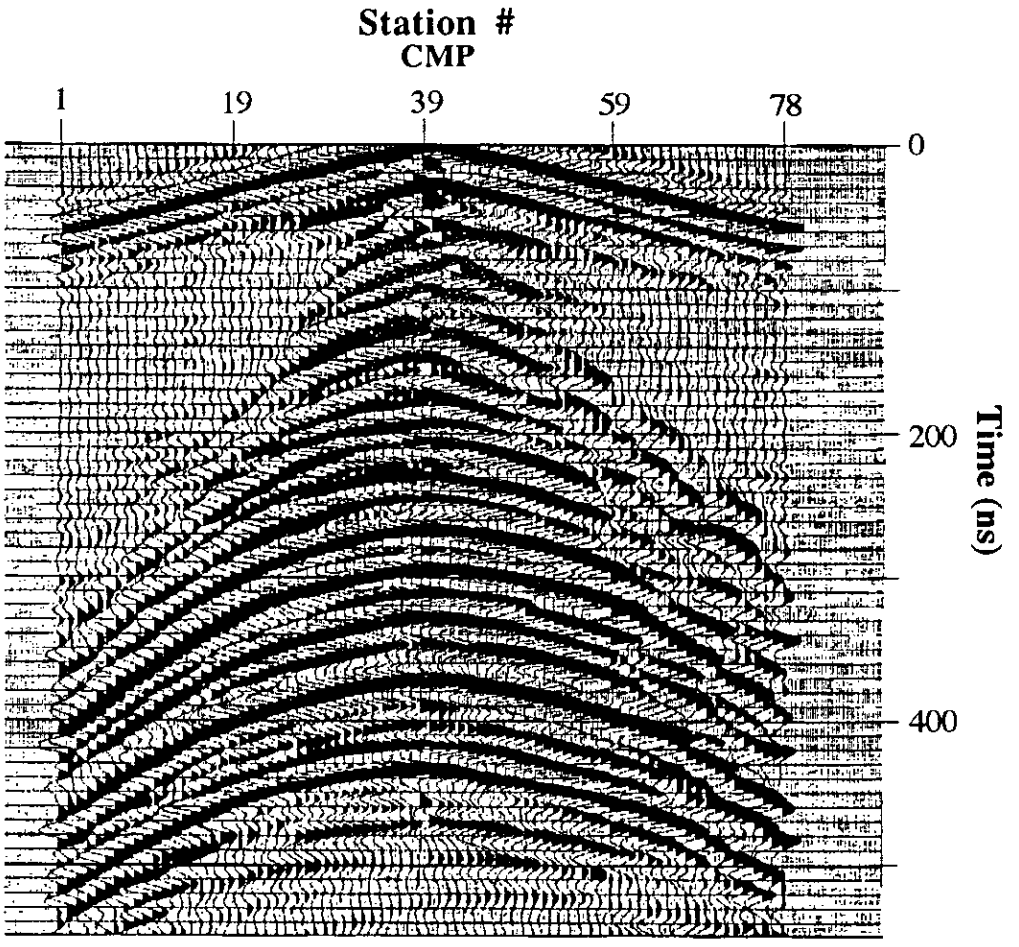

FIG. 10. William's Delta CMP gather. Each trace represents 0.5m transmitter / receiver separation change about the midpoint.

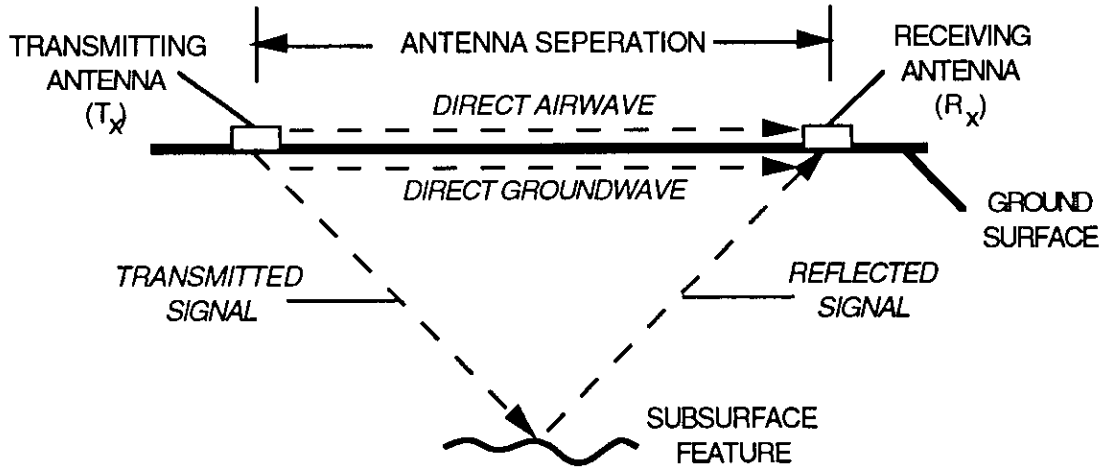

FIG 11. Propagating electromagnectic wave arrivals.

The groundwave is the direct radar pulse travelling through the ground after the airwave (ie second arrival on Figure 6). It's velocity is dependent on surface lithologies and is determined by:

$$V = \frac{\text{source - receiver offset}}{\text{airwave arrival time + (airwave - groundwave traveltimes)}} \quad (3)$$

giving the first radar wave velocity pick on the velocity spectra (Table 1).

Velocity semblance picks for the Figure 10 CMP traces #19 - 59 are shown in Figure 12. The semblance velocity of the direct airwave arrival is plotted at 0.30 m/ns (the speed of light). The radar wave signals transmitted through the ground are the sharp peaks plotted at ~0.070 m/ns. Based on an average radar velocity of ~0.07 m/ns (Table 1) and Jol and Smith's (1991) observation that William's Delta was a water saturated environment, Table 2 suggests the lithology here to be a water saturated, medium / fine sand.

Table 1. Velocity spectra determined from groundwave arrival and velocity semblance analysis.

time t(ns)	velocity($x10^{-3}$ m/ns)
0	63.0
90	71.5
130	72.0
205	72.0
265	71.0
295	75.5
330	71.0
375	69.0
425	68.0

Traces #19 - 59 were used in the velocity semblances because their CMP reflection hyperbolae kept their symmetry and continuity. For highly incident rays (offsets greater than trace #19 and #59 and prior to 200ns) the hyperbolae lose coherency.

Table 2. Table of radar responses for various materials (Davis and Annan, 1989).

MATERIAL	DIELECTRIC CONSTANT	CONDUCTIVITY mS/m	VELOCITY m/ns	ATTENUATION db/M
Air	1	0	0.30	0
Distilled Water	80	0.01	0.033	0.002
Fresh Water	80	0.5	0.033	0.1
Sea Water	80	30000	0.01	1000
Dry Sand	3 - 5	0.01	0.15	0.01
Saturated Sand	20 - 30	0.1 - 1.0	0.06	0.03 - 0.3
Limestone	4 - 8	0.5 - 2	0.12	0.4 - 1
Shale	5 - 15	1 -100	0.09	1 - 100
Silts	5 - 30	1 - 100	0.07	1 - 100
Clays	5 - 40	2 - 1000	0.06	1 - 300
Granite	4 - 6	0.01 - 1	0.13	0.01 - 1
Dry Salt	5 - 6	0.01 - 1	0.13	0.01 - 1
Ice	3 - 4	0.01	0.16	0.01

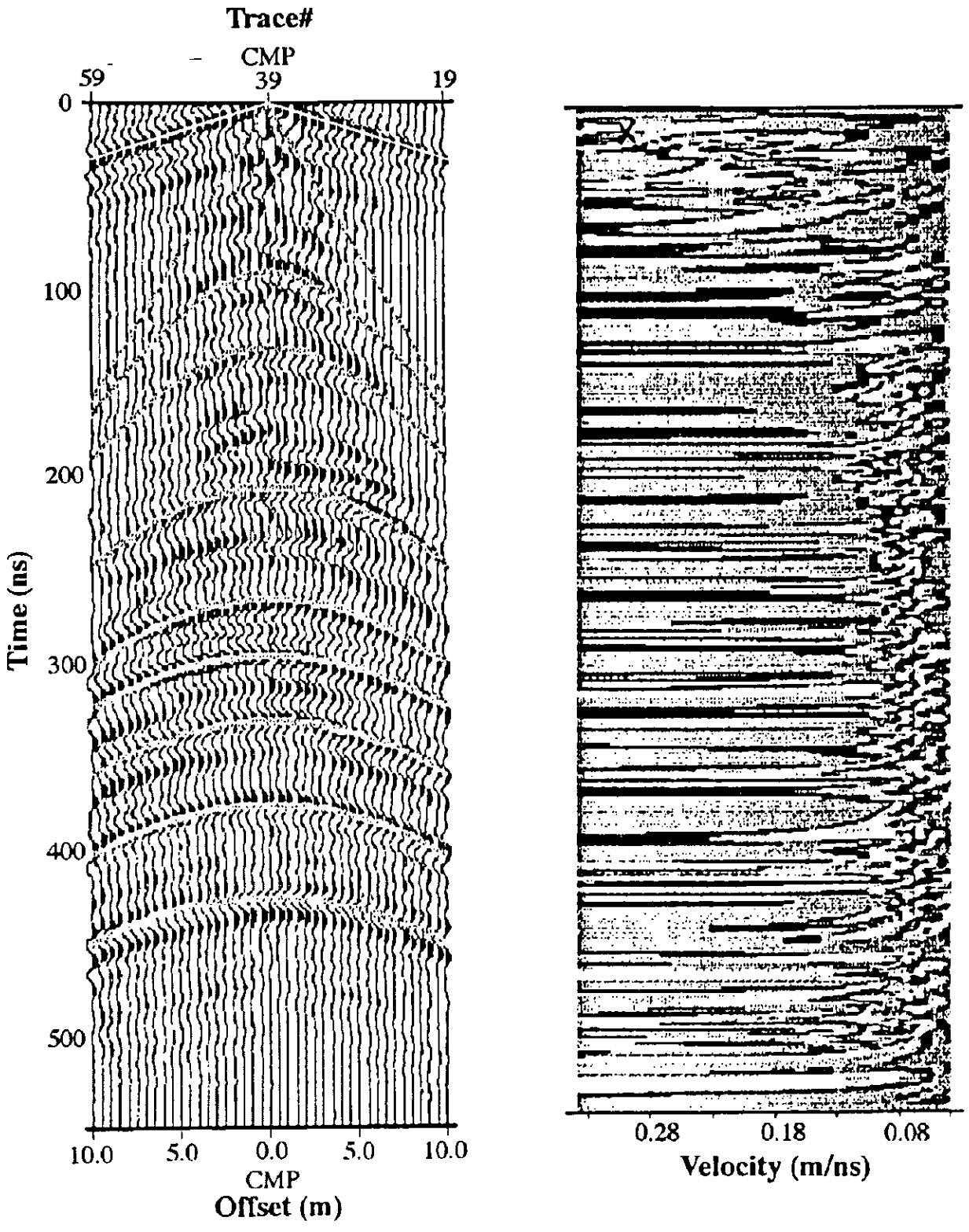

FIG. 12. Velocity semblance plot. Airwave arrival is picked at 0.30m/ns. Transmitted signals plot as peaks at ~0.07 m/ns.

Dielectric constants

Analogous to acoustic impedance in seismic, dielectric constants (K) determine the reflection coefficients for GPR signal reflections (Davis and Annan, 1989):

$$R = \frac{\sqrt{K_1} - \sqrt{K_2}}{\sqrt{K_1} + \sqrt{K_2}}. \tag{4}$$

Thus, assuming a low-loss geological environment, the dielectric is related to electromagnetic velocity (V) according to:

$$V = \frac{c}{\sqrt{K}} \tag{5}$$

where c is the speed of light (c = 0.30 m/ns). For a porous media containing fluid, the porosity (ϕ) is determined from:

$$\sqrt{K} = \phi\sqrt{K}_{fluid} + (1 - \phi)\sqrt{K}_{grain} \tag{6}$$

when $\sqrt{K}_{fluid}$ and $\sqrt{K}_{grain}$ are known experimentally, or from Table 2.

For William's Delta, the earlier velocity analysis found the average radar wave velocity (V) to be ~0.07 m/ns. Therefore, the dielectric constant is from equation (5):

$$K = \left(\frac{c}{v}\right)^2 = \left(\frac{0.30}{0.07}\right)^2 = 18. \tag{7}$$

To determine ϕ, note from Table 2 that $K_{fluid} = 80$ (water), and $K_{grain} \cong 4$ (dry sand). Thus, assuming William's Delta is a water saturated environment:

$$\phi = \frac{\sqrt{K} - \sqrt{K}_{grain}}{\sqrt{K}_{fluid} + \sqrt{K}_{grain}} = \frac{\sqrt{18} - \sqrt{4}}{\sqrt{80} + \sqrt{4}} = 0.33. \tag{8}$$

Elevation corrections

Flattening a GPR profile based on the airwave does not account for near surface elevation and velocity static effects. Therefore, elevation and velocity static corrections should be performed to obtain more realistic subsurface images.

Figure 13 demonstrates the elevation correction. GPR systems measure the travel time of radar waves off subsurface reflectors relative to their position. Assuming a constant radar velocity of 0.07 m/ns, the elevation correction for a topographic low is:

$$\Delta t = \frac{\text{elevation(m)}}{0.07\text{m/ns}} \tag{9}$$

downwards (upwards for a high).

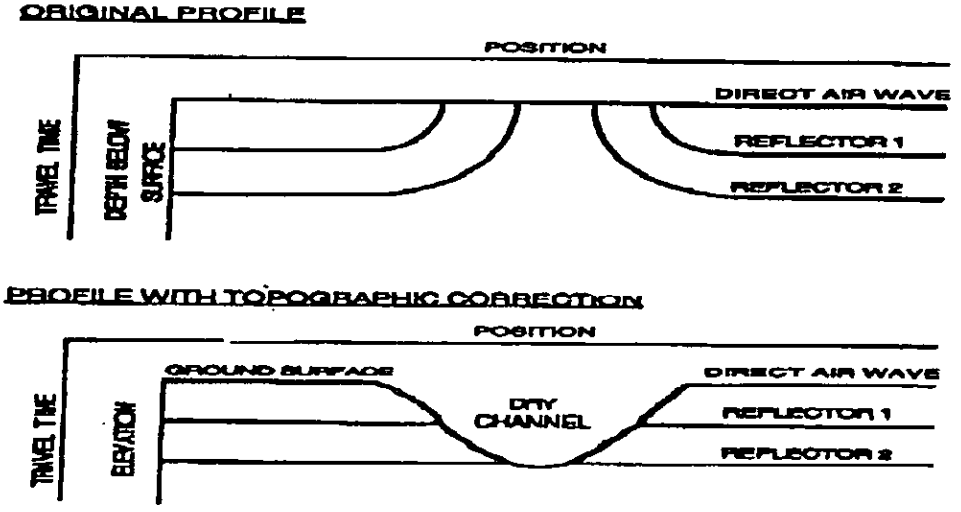

FIG. 13. Schematic illustration of a GPR profile over a dry channel cut through horizontal deposits before and after elevation corrections have been applied (Moorman, 1990).

Static corrections

Velocity static shifts occur when the near surface has significantly different radar velocities than underlying units. In the William's Delta case, two velocity statics were recognized between stations #80-120 and #315-350 (Figure 6 and 15). The velocity push down effect appears to be greater further down in the section for each static. Since no elevation surveys were made for this profile, the statics were water - table flattened (interpreted as the second ground arrival - Figure 15) as an attempt to correct the statics. Figure 14 suggests a further bulk shift of ~10 ns upwards would have been needed for a proper static correction. This is attributed to a significant velocity contrast between dry surficial material overlying water saturated sediments.

In personal communications with Jol and Smith (1991) it was learnt that the William's Delta data set was obtained from a water saturated environment. Inferring the existence of a water table below topographic highs. Also mentioned was the fact that elevation changes accross the section were at most ~1.5-2m.

Knowing that William's Delta is a water saturated environment and the average radar velocity from the velocity semblance analysis was ~0.070 m/ns, Table 2 suggests the lithology to be a water saturated medium/fine sand. Next, the static influenced groundwave arrived earlier than in the surroundings (Figure 15). Suggesting a drier topographic high since the radar velocity of dry sand is substantially higher than wet sand (Table 2). Therefore, this appears to be a case of a velocity static caused by a high velocity surface layer.

When elevation data is available, Figure 16 shows the 2-layer model for an analytical approach to correcting the higher velocity surface layer static problem. Where T_x and R_x are the transmitting and receiving antennae respectively, x is the antenna

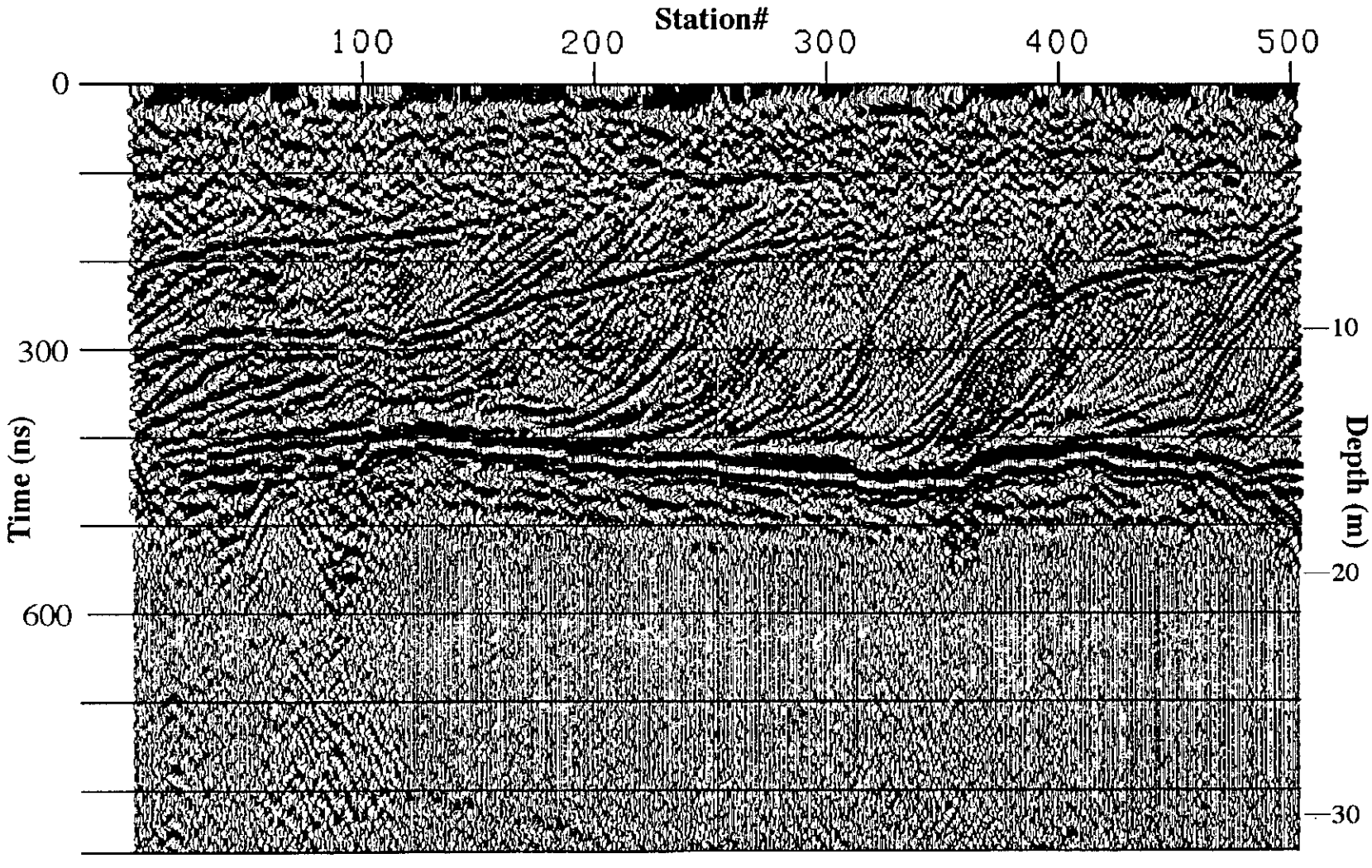

FIG. 14. Groundwave static flattening and normal moveout correction. (Killed trace #252 from 675-850ns).

separation (2m), z_1 is the elevation, z_2 is a subsurface feature's depth below the water table, V_1 is the radar velocity above the water table (≤0.15 m/ns (Table 2) for a dry sand) and V_2 is the approximate velocity below the water level (Table 1 ~0.07 m/ns).

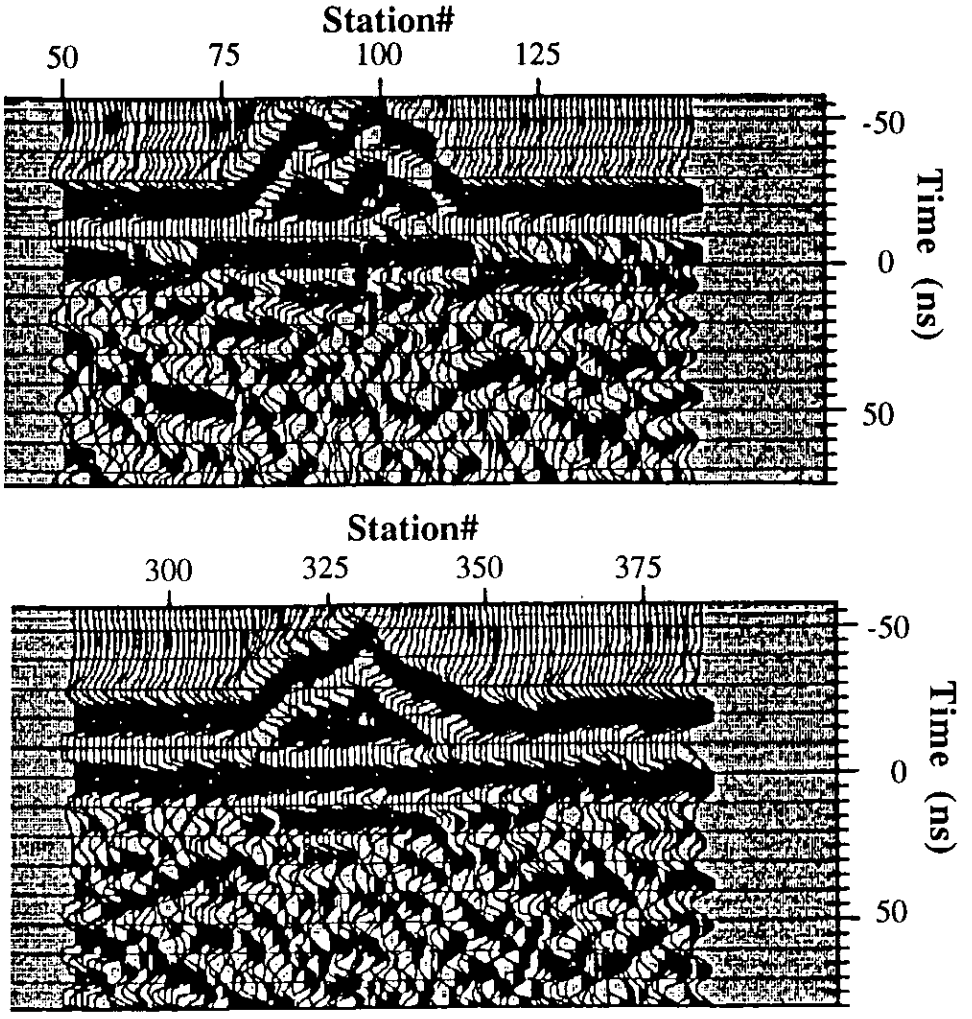

FIG. 15. Velocity static shifts from William's Delta corrected by groundwave flattening.

Next, the major velocity static shifts between stations#80-120 and #315-350 on Figure 7, show the groundwave (the 2nd major arrival) to split in 2. The interpretation of this is that the lower limb of this velocity static "lens" is actually a reflection off the wet sand/dry sand interface (the water table). The 1st layer velocity (V_1) can then be determined from the difference in arrival times between the direct groundwave arrival and the water table reflection (Δt_w).

$$\Delta t_w = 2 \times \sqrt{\left(\frac{x}{2V_1}\right)^2 + \left(\frac{z_1}{V_1}\right)^2} - \frac{x}{V_1} \qquad (10)$$

Arbitrarily taking z_1 = 2m and from Figure 7 the maximum $\Delta t_w \cong$ 25ns:

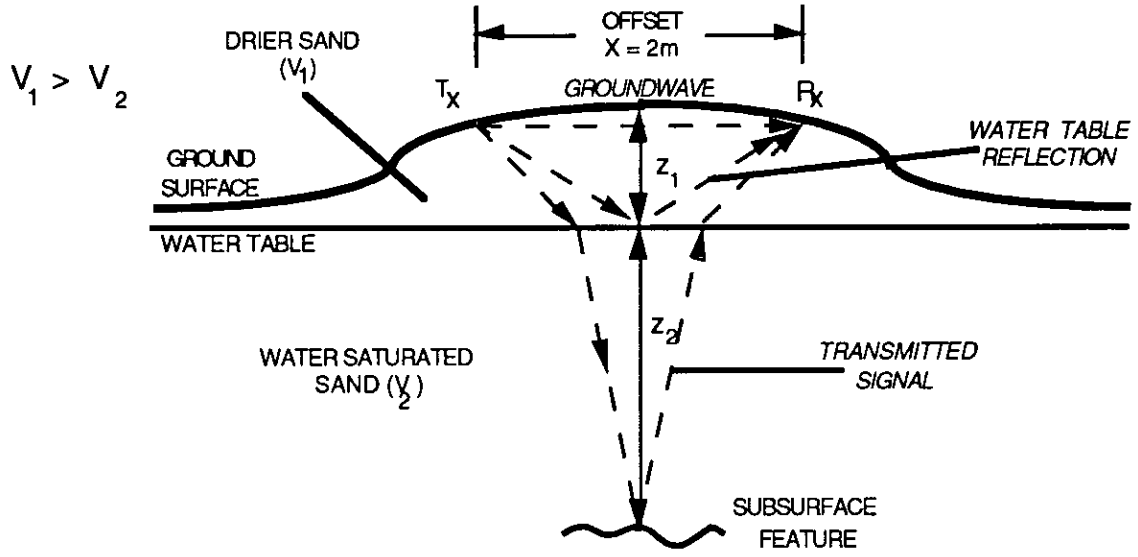

FIG. 16. Diagrammatic representation of the radar signals recognized over the William's Delta velocity statics.

$$V_1 \cong \frac{2}{\Delta t_w} \times \sqrt{\left(\frac{x}{2}\right)^2 + z_1^2}$$

$$\cong \frac{2}{25\text{ns}} \times \sqrt{\left(\frac{2\text{m}}{2}\right)^2 + (2\text{m})^2} \qquad (11)$$

$\cong 0.10$ m/ns (which Table 2 suggests is a drier sand).

These velocity static corrections should be performed before normal moveout (NMO) because it is mathematically simpler. The earlier attempt to resolve the static was done by flattening the water table reflection (see diagram below). Therefore, the bulk static shift for a trace of elevation (z_1) = 2m was ~25 ns. This was found to be insufficient (Figure 14). The ideal velocity static and elevation correction will accomplish the following before NMO (Figure 17). θ_1 and θ_2 are the incident and refracted angles for electromagnetic waves travelling at the velocities V_1 and V_2 respectively, with the horizontal spatial components x_1 and x_2.

From Snell's Law:

$$\frac{\sin\theta_1}{V_1} = \frac{\sin\theta_2}{V_2}, \qquad (12)$$

$$\sin\theta_1 = \frac{x_1}{\sqrt{x_1^2 + z_1^2}} \quad ; \quad \sin\theta_2 = \frac{x_2}{\sqrt{x_2^2 + z_2^2}}. \qquad (13)$$

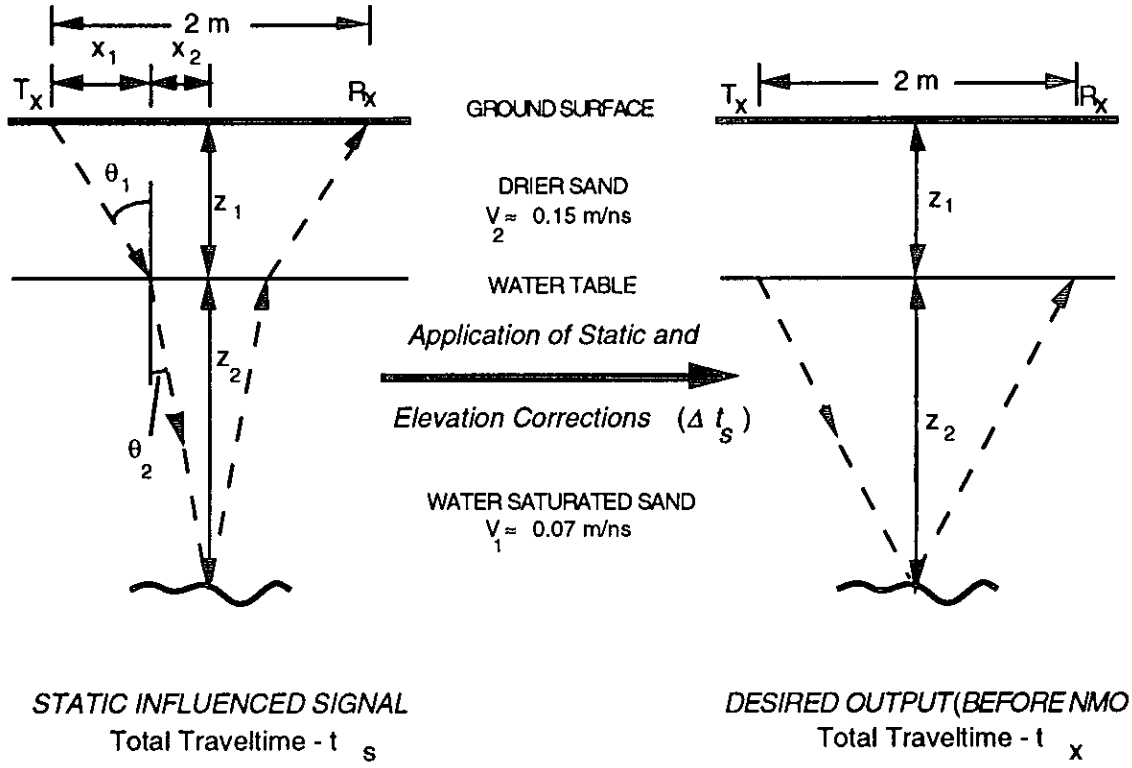

FIG. 17. Diagrammatic representation of velocity static and elevation corrections.

Since the total offset $x = 2m = 2x_1 + 2x_2$ (Figure 17) and thus $x_2 = 1m - x_1$:

$$\frac{V_1}{V_2} = \frac{\sin\theta_1}{\sin\theta_2} = \frac{\dfrac{x_1}{\sqrt{x_1^2 + z_1^2}}}{\dfrac{1-x_1}{\sqrt{(1-x_1)^2 + z_2^2}}} = \sqrt{\frac{1 + \left(\frac{z_2}{1-x_1}\right)^2}{1 + \left(\frac{z_2}{x_1}\right)^2}} \qquad (14)$$

which can be solved for x_1 analytically given V_1, V_2, z_1, and choosing z_2 arbitrarily. Therefore, θ_1 and θ_2 can be derived from equations 12, 13, and 14.

Finally, the static correction (Δt_S) of the total two - way travel time static refracted ray (t_S), to simulate a water table reflected ray (t_X) with antenna separation (x) prior to NMO correction based on Figure 17 is:

$$t_S = \frac{2z_1}{V_1\cos\theta_1} + \frac{2z_2}{V_2\cos\theta_2}; \qquad (15)$$

$$t_X = 2\times\sqrt{\left(\frac{x}{2V_2}\right)^2 + \left(\frac{z_2}{V_2}\right)^2}. \qquad (16)$$

Therefore:

$$\Delta t_S = t_S + t_x = \frac{2z_1}{V_1 \cos\theta_1} + \frac{2z_2}{V_2 \cos\theta_2} - \frac{2}{V_2} \times \sqrt{\left(\frac{x}{2}\right)^2 + z_2^2} \quad . \quad (17)$$

A positive (negative) (Δt_S) signifies an upward (downward) shift in time.

Example

Earlier, flattening the reflection off the water table was tested as a method for correcting the velocity static / elevation shifts. For a station having the maximum elevation (z_1) of ~2m, the bulk static correction (Δt_{Sf}) for that trace was about 25ns upwards (Figures 14 and 15).

Using, equations 12, 13, and 14, to solve for x_1, θ_1 and θ_2 for the arbitrary depths z_2 (=$V_2 \times t_2$ where t_2 is the 2-way vertical travel time through the second layer with velocity V_2), Δt_S is then estimated with equation 16. For the two layer higher velocity surface layer model approximating the velocity static busts in Figure 7, $V_1 \cong$ 0.10 m/ns, $V_2 \cong 0.07$ m/ns, and $z_1 = 2$m are used.

Table 3. Velocity static corrections (Δt_S) approximated using equation 16, choosing $V_1 \cong 0.10$ m/ns, $V_2 \cong 0.07$ m/ns, and $z_1 = 2$m.

z_2	x_1	θ_1	θ_2	Δt_S
15.0m	0.16m	4.6°	3.2°	39.8ns
10.0m	0.22m	6.4°	4.5°	39.8ns
7.5m	0.28m	7.9°	5.5°	39.5ns
5.0m	0.37m	10.4°	7.2°	39.0ns
2.5m	0.54m	15.1°	10.5°	37.1ns
1.0m	0.75m	20.5°	14.2°	31.8ns

In summary, flattening the water table reflection is only a rough estimate (given no elevation data) for correcting the higher surface layer velocity statics seen on the William's Delta GPR line. Equation 16 outlines a more analytical method for correcting this problem.

Normal Moveout

Performed to account for the 2m transmitter / receiver separation using the semblance velocities picked earlier, so traces approximate zero-offset rays.

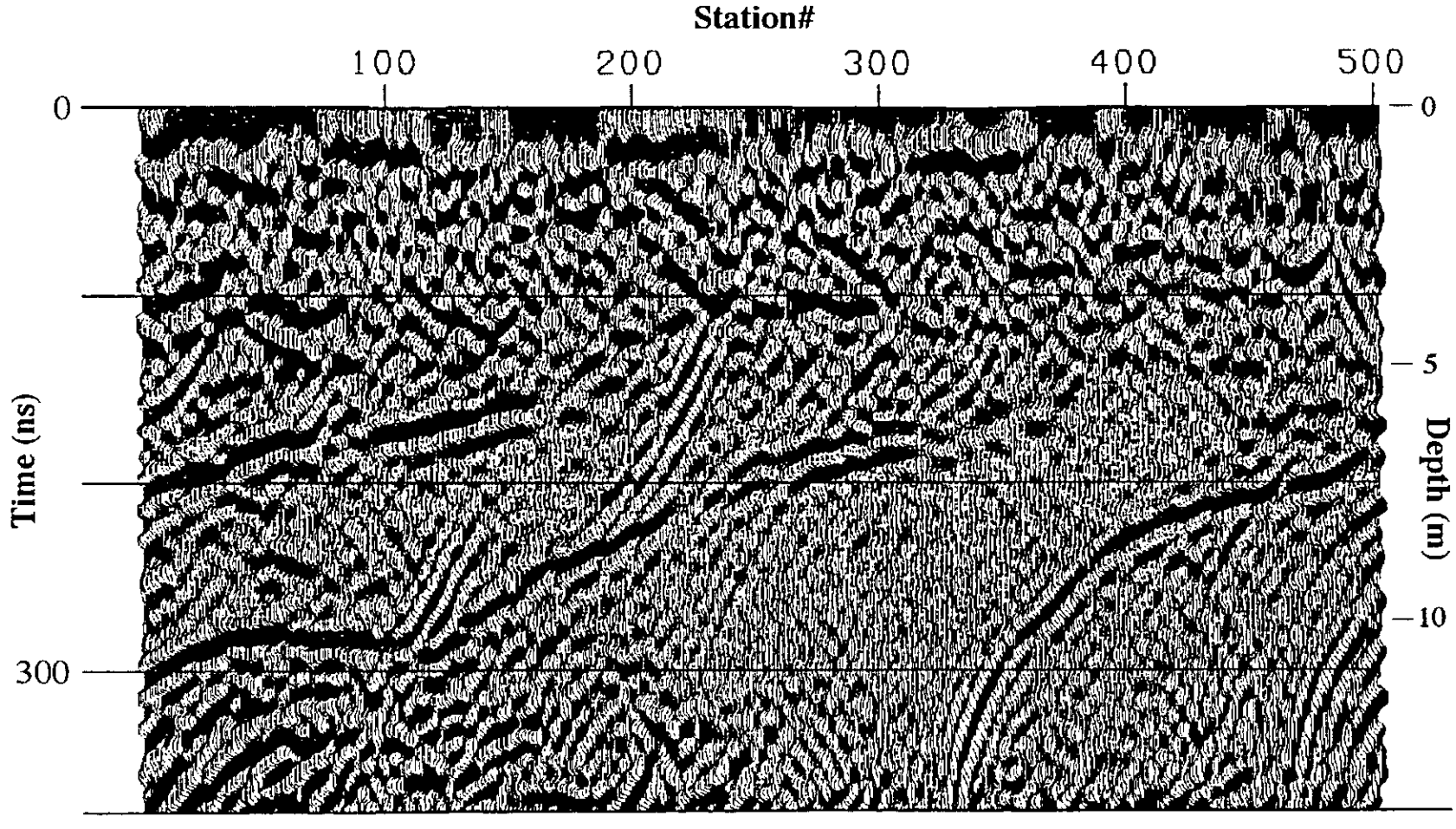

FIG. 18. F - k migrated section (0-375ns).

Migration

Relocates reflections to their true spatial position based on the velocity spectrum to produce a real structure map of subsurface features. The William's Delta data were frequency (f) - wavenumber (k) migrated Figure 18 from 0 to 375ns, because of upward diffraction curves off the strong interface at about 400 ns.

CONCLUSION

The data processing of GPR data is analogous to the processing of seismic data. Using seismic computer software, GPR data processing can better the quality of signal traces and enhance the data's correlatability, continuity, and coherency.

ACKNOWLEDGEMENTS

We would like to thank Dr. Derald Smith of the University of Calgary, Department of Geography for his assistance and access to data.

REFERENCES

Davis, J.L., and Annan, A.P., 1989, Ground-penetrating radar for high-resolution mapping of soil and rock stratigraphy: Geophysical Prospecting, **37**, 531 - 551.

Hogan, G., 1988, Migration of Ground Penetrating Radar Data: a Technique for Locating Subsurface Targets. Proceedings of the Symposium on the Application of Geophysics to Engineering and Environmental Problems, U.S. Geological Survey, Golden, CO. U.S.A., March 28-31. Society of Engineering and Mineral Geophysics, pp. 809-822.

Jol, H. and Smith, D., 1991. Ground Penetrating Radar of Northern Lacustrine Deltas: Canadian Journal of Earth Sciences, **28**, 1939-1947.

Moorman, B.J., 1990. Assessing the Ability of Ground Penetrating Radar to Delineate Subsurface Fluvial Lithofacies, MSc. Thesis, The University of Calgary.

Sensors and Software Inc., 1989, PulseEKKO IV operations manual, p. 66.